ELSEVIER

Journal of Nuclear Materials 274 (1999) 206–217

journal of nuclear materials

www.elsevier.nl/locate/jnucmat

Physical and chemical characteristics of baddeleyite (monoclinic zirconia) in natural environments: an overview and case study

G.R. Lumpkin *

Materials Division, Australian Nuclear Science and Technology Organisation, Private Mail Bag 1, Menai, NSW 2234, Australia

Received 14 October 1998

Abstract

This report provides an overview of the natural occurrence, physical characteristics, and chemical composition of the mineral baddeleyite, ideally ZrO_2. A survey of the literature shows that baddeleyite is widespread in nature as a trace mineral, but has a rather limited composition of 87–99 wt% ZrO_2 with most of the remainder comprised of FeO, TiO_2 and HfO_2. Natural baddeleyite is invariably monoclinic due to the low concentrations of large cations such as Ca and Y. Although the concentrations of Th and U are low (generally <1500 ppm U and <100 ppm Th), the cumulative alpha-decay dose reaches $0.1–1.1 \times 10^{16}$ mg^{-1} for samples with ages of $1–2 \times 10^9$ yr. The available data also suggest that baddeleyite is highly durable in aqueous fluids. For nuclear waste form applications, both the radiation damage effects and durability of baddeleyite need to be examined in further detail. A case study of baddeleyite from the Jacupiranga carbonatite complex of southern Brazil provides some additional information on the crystal chemistry, durability and radiation damage effects of the mineral. This work shows that baddeleyite can incorporate up to 4.1 wt% Nb_2O_5 and 1.2 wt% Ta_2O_5. Incorporation of Nb^{5+} and Ta^{5+} is partially compensated by the incorporation of up to 0.4 wt% MgO and 0.3 wt% FeO in a charge balanced substitution of the form $3Zr \leftrightarrow 2(Nb, Ta) + (Mg, Fe)$. Similar substitution mechanisms may enable the incorporation of Np^{5+} in the ZrO_2 phases of fuel and waste matrices. The mineral is highly resistant to hydrothermal alteration which affected associated uranpyrochlore crystals. Many of the baddeleyite crystals are partially enclosed within the uranpyrochlore grains which contain 19–26 wt% UO_2 and 0.3–3.5 wt% ThO_2. These baddeleyite crystals received maximum alpha-particle doses of $3–4.5 \times 10^{16}$ mg^{-1} within 10 μm of the uranpyrochlore grain boundary, but the intense irradiation has not affected either the structural integrity or the aqueous durability of the mineral.

1. Introduction

Baddeleyite, ideally ZrO_2, is of potential interest as a natural analogue for synthetic ZrO_2 in crystalline ceramic materials designed for the safe disposal of high level nuclear waste from commercial power reactors and, more recently, pure plutonium derived from the decommissioning of strategic nuclear weapons [1–5]. Out of several possible solutions to the disposition of excess weapons Pu, two mainstream approaches have been identified [4]. One approach involves the vitrification of weapons Pu with high level defense wastes at the Savannah River Laboratory followed by underground storage at Yucca Mountain. An alternative to vitrification is the incorporation of weapons Pu into crystalline, titanate ceramic waste forms based on Synroc [6–8]. The major host phases for Pu in these ceramic waste forms are zirconolite and pyrochlore, both of which are anion deficient derivatives of the fluorite structure. The second mainstream approach for the disposition of excess weapons plutonium is the production of a stabilized ZrO_2-based inert matrix fuel for energy production in light water reactors [9].

* Tel.: +61-2 9717 3475; fax: +61-2 9543 7179; e-mail: grl@ansto.gov.au

0022-3115/99/$ – see front matter
PII: S0022-3115(99)00066-5

As demonstrated previously for zirconolite and pyrochlore structure types, natural analogues provide information for the assessment of the long-term performance of ceramic nuclear waste forms primarily in three areas: crystal chemistry, geochemical alteration and radiation damage effects [10–12]. Studies in all three of these areas using natural baddeleyite may provide useful information concerning the long-term performance of monoclinic ZrO_2 in ceramic waste forms. Cubic ZrO_2 is stabilized at low temperatures through the addition of substantial amounts of a cation having a larger ionic radius, for example, Ca^{2+} or Y^{3+} [13,14]. These and other additions lead to the formation of a cubic, anion deficient fluorite phase above a certain critical composition. It is now well known that most of these stabilized defect fluorite compounds exhibit a variety of diffuse scattering effects or superlattice reflections attributable to ordering of cations and vacancies and the development of antiphase domains [15–17]. The usefulness of natural analogue studies for the evaluation of materials such as inert matrix fuel is more restricted due to differences in the composition and structure of baddeleyite and stabilized ZrO_2; however, it is anticipated that at least some application may arise in the areas of crystal chemistry and especially radiation damage effects.

Radiation damage effects in ZrO_2 may vary due to the incorporation of variable amounts of actinides. In general, only the actinide rich cubic form of ZrO_2 in waste forms and inert matrix fuel will undergo substantial internal alpha-decay damage from recoil atoms and alpha particles. However, actinide poor monoclinic ZrO_2 and other phases will undergo alpha particle irradiation from the associated actinide host phases in the waste form. Synthetic ZrO_2 in either the pure monoclinic form or the stabilized cubic form behaves like other fluorite structure types (e.g., CeO_2, ThO_2 and UO_2) and is highly resistant to amorphization by neutrons [18], fission tracks [19], or heavy ions [20]. Monoclinic ZrO_2 when doped with approximately 0.1 wt% UO_2 and subjected to fission fragment damage does, however, undergo a transformation to the cubic modification at fission events doses between 10^{15} and 10^{16} cm^{-3} [19].

The purpose of this report is to present an overview of the available information from the literature on baddeleyite in natural environments, including aspects of the geological occurrence, chemical composition, geochemical alteration and the measurement of U, Th, and Pb isotopes for age dating. This overview is followed by a case study of baddeleyite from the Jacupiranga carbonatite complex of southern Brazil, the principal objectives of which are to extend the data base on natural baddeleyite and address specific questions left unanswered by the literature. New information is presented on the chemistry, aqueous durability and radiation damage effects of the mineral. The paper concludes with a brief discussion of the results and recommendations for future work.

2. Previous work

2.1. Natural occurrence and phase relations

Although baddeleyite is not a common mineral in nature, it is widespread as a trace phase in a wide variety of rock types. The natural occurrences are summarized in Table 1 which includes information about lunar samples, meteorites, tektites and terrestrial rocks [21–26]. In lunar basalts and anorthosites, SNC (of probable Martian origin) meteorites and terrestrial mafic-ultramafic rocks, baddeleyite has been reported as a late stage mineral where it is usually associated with apatite, ilmenite, silicate glass and other accessory phases. The terrestrial examples are notable for the presence of late stage hydrous minerals such as amphibole and mica. These phases may also contain significant amounts of F and Cl and are indicative of a late magmatic fluid phase enriched in volatile elements. All of these igneous rocks probably crystallized at temperatures of about 1100–1500 K and many are silica undersaturated; however, some contain silica glass or quartz [21,22].

Alkaline igneous intrusions such as carbonatites and syenites typically crystallize at temperatures of approximately 900–1200 K and are silica undersaturated. In these rocks, baddeleyite is found as an accessory mineral in association with apatite, calcite, dolomite, magnetite, phlogopite, zirconolite and other minerals [24,25]. Baddeleyite may be replaced by zirconolite or pyrochlore during the late stages of emplacement of carbonatites [24]. In kimberlites, baddeleyite occurs as primary crystals, xenocrysts, or rims on zircon xenocrysts [21,23]. The kimberlite host rocks probably crystallized at temperatures of 1200–1400 K at considerable depth within the lower crust or upper mantle and are silica undersaturated. Baddeleyite has also been reported from silica poor, metacarbonate rocks which formed during regional or contact metamorphism at temperatures on the order of 800–1000 K. In these rocks, baddeleyite occurs in association with calcite, olivine and other accessory minerals.

Allen and Ellis [26] have carried out a theoretical analysis of the stability and phase relations of minerals in the system $CaO–ZrO_2–TiO_2–SiO_2–CO_2$. Their results suggest that baddeleyite may be stable over a wide range of temperature and pressure under crustal and upper mantle conditions. The stability of baddeleyite may extend to very low temperatures in silica undersaturated rocks, where the mineral may occur in association with various combinations of zircon, titanite, calcite, rutile and zirconolite in the presence of a pure CO_2 fluid phase. The theoretical analysis suggests that pure

Table 1
A summary of the natural occurrence and chemical composition (wt%) of baddeleyite

Host rock type	Associated minerals
Lunar basalt	Ilmenite, apatite
Lunar anorthosite	Feldspars, chromite, ilmenite, rutile, zircon, zirconolite, apatite, pyroxene, silicate glass
SNC meteorites	Ilmenite, magnetite, pyrrhotite, whitlockite, quartz, olivine, apatite, silicate glass
Tektites	Silicate glass, zircon
Mafic–ultramafic rocks	Amphibole, biotite, chlorite, quartz, feldspars, apatite, ilmentite, spinel, chalcopyrite, zircon, zirconolite
Alkaline intrusions	Apatite, calcite, ilmenite, pyroxene, amphibole, olivine, magnetite, pyrochlore, thorianite, zircon, zirconolite
Kimberlites	Zircon, pyroxene, zirconolite, magnetite, rutile, ilmenite, perovskite, garnet
Metacarbonates	Zirconolite, calcite, olivine, geikielite

	Lunar basalts			Mafic–ultramafic rocks			Metacarbonatites		
	Ave.	Min.	Max.	Ave.	Min.	Max.	Ave.	Min.	Max.
Nb_2O_5	0.8	0.6	1.1	0.4	–	–	0.4	0.2	0.9
SiO_2	0.2	0.1	0.3	0.1	0.0	0.2	–	–	–
ZrO_2	92.5	87.2	94.8	97.0	92.5	98.7	96.9	95.0	99.0
TiO_2	3.2	1.3	8.0	1.1	0.1	2.6	0.7	0.0	1.7
HfO_2	2.0	1.6	2.6	1.5	0.9	2.2	1.8	1.0	2.5
Al_2O_3	0.3	0.1	0.6	0.1	0.0	0.2	–	–	–
Cr_2O_3	0.2	0.1	0.3	0.1	0.0	0.2	–	–	–
Y_2O_3	1.4	1.2	1.5	0.1	0.0	0.3	0.2	0.0	0.3
MgO	0.1	0.0	0.2	0.1	0.0	0.3	–	–	–
CaO	0.3	0.1	0.6	0.1	0.0	0.4	0.4	0.0	0.9
MnO	0.1	0.0	0.2	<0.1	0.0	0.1	–	–	–
FeO	1.1	0.4	2.1	0.8	0.0	2.2	0.6	0.1	2.2

baddeleyite is not thermodynamically stable in the presence of quartz over the range of conditions investigated, providing an explanation for the rarity of the mineral in nature. However, as noted above, there are exceptions to this rule which indicate that baddeleyite may have a greater range of stability in more complex systems.

2.2. Chemical composition

Very few high quality analyses have been reported for natural baddeleyite. Using the available data from the literature [21,23,24], a summary of the chemical composition of baddeleyite from various natural occurrences is presented in Table 1, including an unweighted average, minimum and maximum value for each reported oxide. This summary indicates that the mineral generally contains 87–99% ZrO_2 by weight. Analyses show that the major impurities found in baddeleyite are 0.1–8.0 wt% TiO_2, 0.9–2.6 wt% HfO_2 and 0.0–2.2 wt% FeO. The relatively high concentrations of TiO_2 and FeO reported for baddeleyite are generally restricted to examples from more highly evolved mafic–ultramafic igneous rock types with bulk compositions characterized by high Fe/Mg + Fe ratios and elevated concentrations of minor elements (e.g., K, Ti and Mn). Preferential incorporation of Ti and Fe may expand the stability field of baddeleyite relative to zircon, providing a possible explanation for the coexistence of baddeleyite and quartz in Fe rich bulk rock compositions.

Significant amounts of other elements are generally restricted to lunar basalts, where maximum levels of 1.5 wt% Y_2O_3 and 1.1 wt% Nb_2O_5 have been reported. Maximum concentrations of other elements are 0.3 wt% MgO, 0.6 wt% Al_2O_3, 0.4 wt% SiO_2, 0.8 wt% CaO, 0.3 wt% Cr_2O_3 and 0.2 wt% MnO. Some of these elements may be overestimated due to fluorescence of surrounding mineral phases during electron probe analysis of micrometer sized baddeleyite crystals, especially Al_2O_3, SiO_2 and CaO which are major components of the host rock. Trace element analyses indicate that baddeleyite contains 30–510 ppm Pb, 2–70 ppm Th and 160–1400 ppm U by weight [21].

2.3. Geochemical alteration

Most of the available information on the chemical durability of baddeleyite pertains to reactions that occur during the crystallization and differentiation of high temperature igneous liquids with crystallization temperatures of 900–1500 K, depending on rock type and bulk composition. In most cases, the magmatic replacement of baddeleyite at high temperatures involves reaction of baddeleyite with liquid to produce either zircon or, less

commonly, zirconolite reaction rims. Similar observations have been made on metamorphic rocks where the mineral assemblage may change as a function of pressure, temperature and fluid composition. It is now reasonably well established that baddeleyite reacts with an aqueous fluid phase to form zircon under conditions of elevated silica activity during regional metamorphism under conditions ranging from greenschist to granulite facies [21]. Metamorphic reaction of baddeleyite with fluid occurred at estimated temperatures of 650–1100 K, depending on lithostatic pressure [27].

Information on low temperature, aqueous durability in natural environments is virtually non-existent. However, at least one study has suggested that baddeleyite can react with aqueous fluid to produce zircon during a very late stage, low temperature alteration event [21]. In this example, the temperature at which the alteration occurred is not well constrained, but is probably below 575–625 K based on the available information [27]. Baddeleyite is also known to occur in placer deposits formed by the weathering and complete break down of the host rock. Perhaps the best example is the occurrence of baddeleyite in stream gravels of Sri Lanka, together with corundum, zircon, zirconolite and other minerals resistant to chemical and physical breakdown. Experimental studies have shown that baddeleyite is highly insoluble in aqueous fluids, but the solubility varies as a function of pH, having a characteristic v-shaped pattern [9]. The solubility of baddeleyite is about 10^{-3} M under highly acidic conditions (pH = 1), dropping to a minimum of approximately 10^{-12} M at pH values of 5–7, and increasing to about 10^{-3} M for highly basic conditions (pH = 13–14). The potential effects of low temperature alteration and metamorphism on U–Th–Pb isotope systematics are discussed further in Section 2.4.

2.4. U–Th–Pb isotopes and age dating

Heaman and LeCheminant [21] have provided a detailed description of the procedures required to recover clean baddeleyite fractions for age dating and presented results from several case studies. The examples summarized here are significant because of the geological time scales involved (0.9–2.2 Ga). In the first example, nine fragments of a large single crystal of baddeleyite from the Phalaborwa carbonatite complex of South Africa were analyzed using a thermal ionization mass spectrometer. Results indicated that 2σ analytical precision of ±0.092% for $^{206}Pb/^{238}U$, ±0.086% for $^{207}Pb/^{235}U$, and ±0.008% for $^{207}Pb/^{206}Pb$ was achieved despite variations in the U content of 292–1389 ppm. All of the analyses are less than 1% discordant, consistent with closed system behavior with respect to Pb loss or U gain. The resulting average $^{207}Pb/^{206}Pb$ age of 2059.8 ± 0.8 Ma is consistent with previous age dating of the Phalaborwa complex [28]. The precision of the baddeleyite dating technique was further illustrated using samples from the extensive Mackenzie diabase dike swarm of northern Canada. In this example, the $^{207}Pb/^{206}Pb$ ages of nine samples ranged from 1265 to 1272 Ma with seven of the samples giving ages of 1267 or 1268 Ma.

Additional examples were reviewed by Heaman and LeCheminant [21] in order to document the effects of alteration and metamorphism on the U–Th–Pb isotope systematics of baddeleyite. The Saratoga Springs gabbro sill of the Death Valley region, California, has well preserved primary igneous textures, but some samples also exhibit both a high temperature alteration mineral assemblage caused by reaction with late magmatic fluids and a low temperature alteration assemblage. Three U–Pb analyses of baddeleyite from the sill are between 11% and 19% discordant and define a line with an upper intercept age of 1069 ± 3 Ma and a lower intercept age of 65 Ma [29]. The two intercept ages probably represent the crystallization age and time of low temperature alteration, respectively. The discordance of the baddeleyite samples is not due to Pb loss, but is related instead to the presence of botryoidal zircon overgrowths which formed during the low temperature alteration event [21,29].

In the Hurwitz gabbro sills of the Northern Territories of Canada, metamorphic zircon reaction rims developed on baddeleyite during greenschist facies metamorphism [21,30] (estimated temperatures are 625–825 K, depending on pressure [27]). Three U–Pb analyses showed discordance of 12–31% which correlated directly with the abundance of metamorphic zircon. An upper intercept age of 2094 Ma was derived from these data, consistent with a concordant age of 2111.2 ± 0.6 Ma determined from another group of baddeleyite samples with limited zircon growth (the age of metamorphism was difficult to determine due to Pb loss from the zircon reaction rims). Finally, in gabbro samples of the Grenville province of eastern Canada, polycrystalline zircon reaction rims of variable thickness formed on baddeleyite during high grade metamorphism from middle amphibolite to granulite facies [21,31] (estimated temperatures are 900–1100 K [27]). These studies demonstrate that magmatic baddeleyite and zircon give consistent U–Pb crystallization ages of 1150–1152 Ma, polycrystalline zircon aggregates give ages of 1046–1060 Ma for the Grenville metamorphic event, and mixed samples with metamorphic zircon reaction rims give ages that scatter between the two extremes.

2.5. Radiation damage effects

The alpha-decay dose and displacements per atom (dpa) have been calculated for baddeleyite in three of the case studies summarized above using the range of measured U and Th concentrations and the crystallization age by using the following equations:

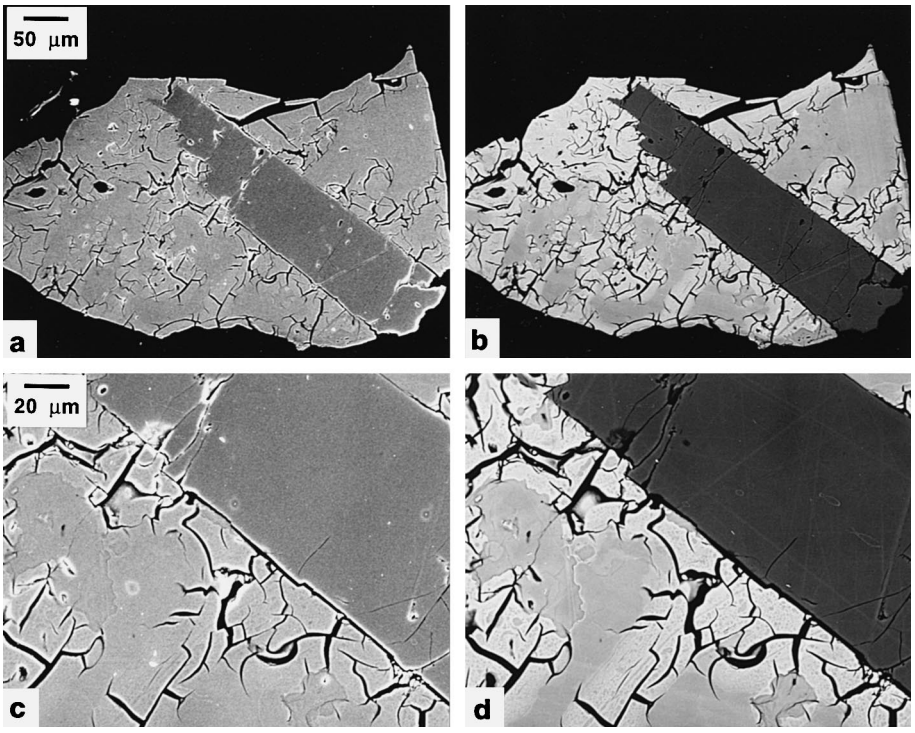

Fig. 1. Secondary electron (a, c) and backscattered electron image (b, d) pairs of an intergrowth between uranpyrochlore and baddeleyite from the Jacupiranga carbonatite complex, Brazil. Images taken at low magnification (a, b) show the general features, including microfracturing and alteration in the uranpyrochlore (lighter gray) and the platy habit of the baddeleyite (darker gray). Note the embayment of baddeleyite at the top of the images. Higher magnification images (c, d) show details of alteration in the uranpyrochlore and absence of alteration in the baddeleyite.

$$D = 6 \cdot N_{232_{Th}} \cdot (e^{\lambda 232_{Th} \cdot t} - 1) + 8 \cdot N_{238_U} \cdot (e^{\lambda 238_U \cdot t} - 1) \quad (1)$$

$$\text{dpa} = \frac{1500 \cdot D \cdot M_f}{N_A \cdot N_f}. \quad (2)$$

In Eq. (1), $N_{232_{Th}}$ and N_{238_U} represent the present numbers of atoms of ^{232}Th and ^{238}U, $\lambda_{232_{Th}}$ and λ_{238_U} are their decay constants, and t is the geological age. Note that no consideration was given to the presence of ^{235}U which accounts for a very small fraction of the total U concentration. In Eq. (2), M_f is the molecular weight of one formula unit, N_A is the Avagadro constant, and N_f is the number of atoms per formula unit.

For baddeleyite from the Phalaborwa carbonatite, the calculated cumulative alpha-decay dose ranges from 0.19×10^{16} to 0.98×10^{16} mg^{-1}, corresponding to 0.20–1.01 dpa (assuming 1500 atomic displacements per alpha-decay event, see the case study below for further information). Baddeleyite samples from the Hurwitz gabbro have calculated alpha doses of $0.47–0.68 \times 10^{16}$ mg^{-1} (0.49–0.70 dpa) and the single pure baddeleyite sample from the Grenville coronitic gabbro has a calculated alpha dose of 0.064×10^{16} mg^{-1} (0.07 dpa). Unfortunately, the crystallinity of the natural baddeleyite samples summarized above is not specifically stated [21], emphasizing the need for further studies of radiation damage effects and the possible consequences for aqueous durability and age dating.

The cumulative alpha-decay doses calculated for the three examples discussed above do not appear to have any systematic relationship with the levels of discordance or metamorphic history of the samples [21]. Generally speaking, the geological age dating studies have not considered the potential effects of radiation damage on the U–Th–Pb isotope systematics. This may be due to the tendency of baddeleyite to retain a high degree of crystallinity in spite of cumulative dose levels that cause severe structural damage in other oxide and silicate minerals (e.g., pyrochlore, zirconolite and zircon [10]). Earlier heavy ion irradiation experiments have identified ZrO_2, along with several other compounds having the fluorite structure, as belonging to a class of materials that remain crystalline to doses in ion excess of 10^{17} cm^{-2} [32]. This dose is at least 2–3 orders of magnitude greater than the critical amorphization doses of other actinide host phases in ceramic nuclear waste forms, including perovskite, pyrochlore, zircon and zirconolite.

3. Case study

The literature survey presented above primarily illustrates the range of chemical composition, U–Th–Pb isotope systematics, and stability of baddeleyite at moderate to high temperatures. There are several topics that remain to be addressed, including the interpretation of substitution mechanisms, stability at lower temperatures, and effects of radiation damage on the physical and chemical properties of baddeleyite. These topics are examined in greater detail in Sections 3.1–3.5.

3.1. Sample description

The samples described in this section are from the Jacupiranga carbonatite complex of southern Brazil. The igneous complex has an age of approximately 130 Ma and consists of a series of magnesian silicate (pyroxenite, peridotite, etc.) rocks with subordinate carbonatite intrusions in the core of the complex [33]. Baddeleyite has been found in the pyroxenite and carbonatite rocks of the intrusive complex. In the pyroxenite, baddeleyite is associated with pyroxene, amphibole, ilmenite, clinohumite and zirconolite. The baddeleyite samples investigated in this work are from the author's personal collection and from a small research collection in the the Department of Geology, University of New Mexico. Baddeleyite crystals in these samples are associated with small (~1 mm) uranpyrochlore crystals recovered from carbonatite. The baddeleyite occurs as colorless, flat plates or blades either intergrown with uranpyrochlore or more rarely, as millimeter to submillimeter single crystals or twinned crystals with no associated uranpyrochlore. Examples of the intergrowths with uranpyrochlore are shown in Figs. 1 and 2. These images reveal that the baddeleyite crystal morphology can be quite variable, especially within the confines of the uranpyrochlore host, where curved grain boundaries and embayments are common (Fig. 1(a, b) and Fig. 2(a, b)). Kapustin [24] has reported similar associations of baddeleyite and pyrochlore group minerals from several carbonatite complexes in the Kola peninsula of northeastern Russia.

3.2. Experimental procedures

Only a brief summary of the experimental methods are given here as most of the details can be found elsewhere [34,35]. Investigations using scanning electron microscopy (SEM) and energy dispersive microanalysis

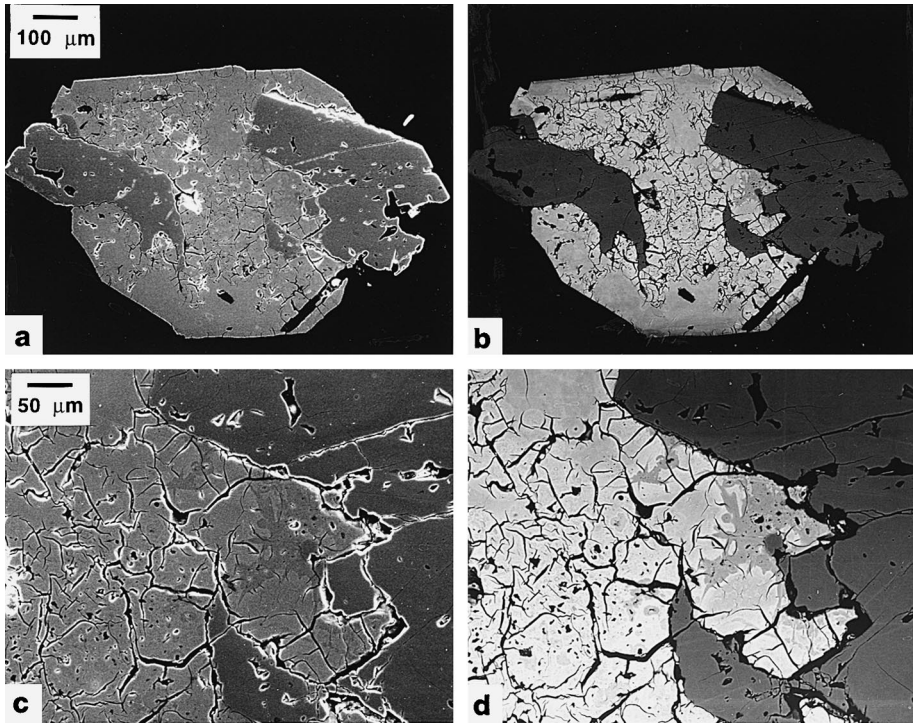

Fig. 2. Secondary electron (a, c) and backscattered electron image (b, d) pairs of another intergrowth between uranpyrochlore and baddeleyite. Images taken at low magnification (a, b) illustrate euhedral morphology of the uranpyrochlore (lighter gray) and the irregular morphology and embayment of the baddeleyite (darker gray). Higher magnification images (c, d) show details of microfracturing and alteration.

(EDX) were carried out using a JEOL 6400 SEM equipped with a Noran EDX detector. Petrographic observations were augmented with secondary and backscattered electron images and specific areas of interest were checked by EDX. Standardless analyses of uranpyrochlore and baddeleyite were acquired for 500 s and processed using Tracor software. The EDX analyses were optimized by calibrating against minerals and compounds of known composition. Operating conditions for the analyses were 25 kV and 1 nA probe current.

Quantitative electron probe microanalyses (EPMA) were obtained using a JEOL 733 Superprobe operated at 15 kV and 20 nA probe current. Data were corrected for drift, deadtime and reduced to weight percent oxides using empirical correction factors. Each element was counted for 40 s or until a standard deviation of 0.5% was reached. Peak interference problems were addressed using a set of empirical overlap correction factors. Standards for the analyses included well characterized silicate and oxide minerals and a set synthetic binary oxide single crystals (see Ref. [34] for further details).

Analytical electron microscopy (AEM) investigations were carried out using a JEOL 2000 FXII electron microscope operated at 200 kV and equipped with a Link ISIS EDX system. Electron diffraction work was carried out using a nominal camera length of 80 cm. For accurate measurement of d-spacings, the instrument has been calibrated at this camera length for a range of objective lens current settings using a gold standard. EDX analyses were generally acquired for 300 s and processed using a digital top-hat filter to remove the background, a multiple least squares fitting routine to determine the peak counts, and a set of experimental k-factors determined from a large suite of silicate and oxide reference materials (see Ref. [35]).

3.3. Chemical composition

Results of the SEM-EDX and EPMA analyses are given in Table 2. These data demonstrate that in carbonatites, Nb_2O_5 and Ta_2O_5 can be present in baddeleyite in significant amounts, in this case up to maximum values of about 4.1 and 1.2 wt%, respectively. Typical of other baddeleyite samples (see analyses listed in Table 1), these crystals contain between 0.6 and 1.4 wt% HfO_2. Concentrations of other elements are low, with maximum amounts of 0.1 wt% TiO_2, 0.3 wt% UO_2, 0.1 wt% Y_2O_3, 0.1 wt% Ce_2O_3, 0.3 wt% MgO, 0.2 wt% CaO and 0.3 wt% FeO detected. Other oxides, including SiO_2, ThO_2, Al_2O_3 and MnO were near or below their respective detection limits for the SEM-EDX and EPMA techniques. The low concentration of TiO_2 in baddeleyite from the Jacupiranga carbonatite (compare Tables 1 and 2) is interesting and probably reflects the bulk composition of the host rock. This suggestion is consistent with the composition of associated uranpyrochlore in which the concentration of ZrO_2 (1.2–2.0 wt%) exceeds that of TiO_2 (0.4–1.2 wt%).

Calculated formulae of baddeleyite, based on a total of two oxygen atoms per formula unit, show that the mineral contains between 0.92 and 1.00 Zr atoms per formula unit (pfu) with most of the remainder accounted for by Nb, Ta, Hf, Mg and Fe (Table 2). Of this group, Hf is relatively constant from point to point and only accounts for 0.004–0.008 atoms pfu of the available cation sites. Most of the variation in composition is due to core to rim variations in the amounts of Nb, Ta, Mg and Fe, which attain maximum concentrations of 0.038, 0.007, 0.008 and 0.004 atoms pfu, respectively. The compositional variation is not consistent from grain to grain, with some crystals having Nb-rich rims whereas others have Nb-poor rims. In all cases, the cation totals are within ±0.5% of the ideal value of one, indicating that the natural baddeleyite crystals conform to MO_2 stoichiometry.

Results of the analyses are plotted in Fig. 3 and provide strong evidence for the correlated substitution of Zr for Nb, Ta, Mg and Fe. A plot of [Zr] vs. [Nb] + [Ta] + [Mg] + [Fe] (Fig. 3(a)), with [*X*] the atom number of *X* for 2 oxygen atoms, shows an excellent negative correlation with both the SEM-EDX and EPMA data lying close to the same trend. Linear regression analyses were performed on the individual data sets and gave the following results:

$$[\mathrm{Nb}] + [\mathrm{Ta}] + [\mathrm{Mg}] + [\mathrm{Fe}] = 0.956 - 0.965 \cdot [\mathrm{Zr}],$$
with $r = 0.998$ for the EPMA data

$$[\mathrm{Nb}] + [\mathrm{Ta}] + [\mathrm{Mg}] + [\mathrm{Fe}] = 0.941 - 0.947 \cdot [\mathrm{Zr}],$$
with $r = 0.992$ for the SEM-EDX data

Although the two data sets represent baddeleyite crystals with slightly different composition ranges, they define regression lines that are virtually identical. The substitution mechanism responsible for this trend was investigated further and it was found that a plot of [Nb] + [Ta] vs. [Mg] + [Fe] (Fig. 3(b)) exhibits a good positive correlation. Linear regression analyses gave the following results:

$$[\mathrm{Mg}] + [\mathrm{Fe}] = -0.0022 + 0.488 \cdot ([\mathrm{Nb}] + [\mathrm{Ta}]),$$
with $r = 0.988$ for the EPMA data

$$[\mathrm{Mg}] + [\mathrm{Fe}] = -0.0003 + 0.523 \cdot ([\mathrm{Nb}] + [\mathrm{Ta}]),$$
with $r = 0.981$ for the SEM-EDX data

In this case, the two data sets define slightly different regression lines and it appears that the EPMA data are shifted systematically to higher [Nb] + [Ta] values (Fig. 3(b)), possibly as a consequence of a poor choice of background positions. Nevertheless, both data sets define trends with slopes of approximately 0.5. The statistics shown above are consistent with a substitution of

Table 2
Electron microbeam analyses (wt%) and chemical formulae (atoms of X per 2.000 oxygens: [X] At/2O) of natural baddeleyite from carbonatite, Jacupiranga, Brazil

Sample analysis	Py12-3 bd3c	Py12-3 bd3r	Py12-5 bd5c	Py12-5 bd5r	325 bd1	325 bd11	325 bd5	325 bd7
Wt%								
Nb_2O_5	2.6	1.8	1.1	<0.2	0.59	2.76	3.63	4.03
Ta_2O_5	0.1	0.3	0.4	<0.1	0.18	0.93	0.90	0.82
ZrO_2	95.4	96.6	96.9	99.0	96.8	94.0	92.0	92.0
TiO_2	0.10	0.06	0.05	<0.05	<0.03	0.04	0.05	<0.03
HfO_2	1.2	0.6	0.9	0.8	1.29	1.33	1.17	1.24
UO_2	<0.1	0.1	0.3	<0.1	0.11	0.09	0.08	0.08
MgO	0.22	0.27	0.12	<0.05	<0.03	0.23	0.34	0.38
CaO	0.08	0.04	0.19	<0.04	<0.03	<0.03	<0.03	<0.03
FeO	0.29	0.18	0.13	<0.06	<0.05	0.31	0.44	0.41
sum [a]	99.99	99.95	100.09	99.80	98.97	99.79	98.71	98.99
[X] At/2O								
Nb	0.024	0.017	0.010	0.000	0.006	0.026	0.034	0.038
Ta	0.001	0.002	0.002	0.000	0.001	0.005	0.005	0.005
Zr	0.954	0.954	0.966	0.972	0.984	0.945	0.933	0.930
Ti	0.002	0.001	0.001	0.000	0.000	0.001	0.001	0.000
Hf	0.007	0.004	0.005	0.005	0.008	0.008	0.007	0.007
U	0.000	0.000	0.001	0.000	0.001	0.000	0.000	0.001
Mg	0.007	0.008	0.004	0.000	0.000	0.007	0.011	0.012
Ca	0.002	0.001	0.004	0.000	0.000	0.000	0.000	0.001
Fe	0.005	0.003	0.002	0.000	0.000	0.005	0.008	0.007
Total	1.001	1.002	1.002	1.000	0.998	0.999	0.999	0.999

[a] SiO_2, Al_2O_3, Y_2O_3, Ce_2O_3, and MnO were sought, but not detected.

the form $3Zr \leftrightarrow 2(Nb, Ta) + (Mg, Fe)$. These observations suggest that a columbite-like component, $(Mg, Fe)(Nb, Ta)_2O_6$, is soluble in baddeleyite up to a maximum of about 6 mol%.

3.4. Geochemical alteration

As noted above, many of the baddeleyite crystals examined in this study are intergrown with uranpyrochlore. Although a complete description of the uranpyrochlore is beyond the scope of this paper, it is of direct interest to note that many of the uranpyrochlore crystals exhibit hydrothermal alteration. Based on petrographic criteria, Lumpkin and Ewing [36] have suggested that the alteration is of the 'primary' hydrothermal type in which the rims of the uranpyrochlore crystals exchanged certain elements with an aqueous fluid phase at elevated temperatures. Typically, the altered rims are depleted in Ca, Na and F and enriched in Fe, Sr and Ba. The precise conditions of alteration are not known; however, Lumpkin and Ewing [36] suggested that primary alteration in carbonatites occurred at maximum temperatures of 725–825 K based on sub-solidus silicate mineral reactions. Similar hydrothermal activity may extend to even lower temperatures in carbonatites (approximately 475–625 K) and is usually characterized by lower activities of HF, Na and Ca and elevated activities of Fe, Sr and Ba.

Further studies of the uranpyrochlore have been carried out in order to document the alteration environment of the associated baddeleyite. Some examples of the alteration are illustrated in Figs. 1 and 2. The SEM images shown here reveal that the uranpyrochlore host phase contains irregular, microfractured zones of alteration. SEM-EDX analyses of unaltered and altered areas generally show that the alteration involved removal of Na by the fluid phase, accompanied in some areas by minor depletion in Ca. The behavior of Fe, Sr and Ba is erratic, but in some areas they appear to increase in the altered regions of the sample. A significant feature of the uranpyrochlore is that the Th and U concentrations remain unaffected by the alteration, confirming earlier work [36]. In every intergrowth examined, the associated baddeleyite crystals do not appear to have been affected by the alteration (Fig. 1(c, d) and Fig. 2(c, d)). SEM images of the uranpyrochlore and baddeleyite show that the baddeleyite is relatively unfractured and has uniform contrast. There is no evidence for alteration along any of the existing fractures in the baddeleyite, even though the aqueous fluid phase clearly had access to these areas. The baddeleyite immediately adjacent to the grain boundary is also

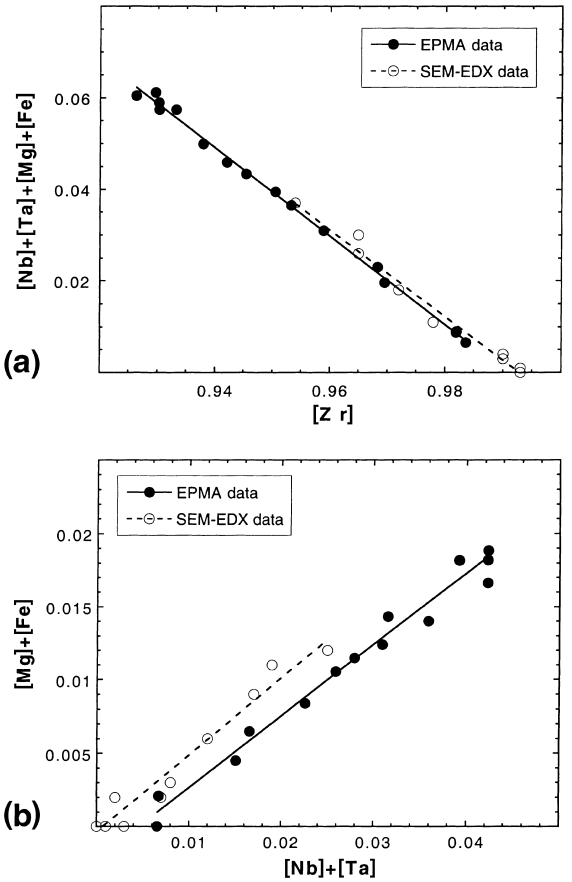

Fig. 3. Plots of the chemical composition of baddeleyite from Jacupiranga, Brazil. (a) Plot of [Nb] + [Ta] + [Mg] + [Fe] vs. [Zr]. Approximate 1:1 correlation demonstrates that Nb, Ta, Mg, and Fe substitute as a group for Zr in the structure of natural baddeleyite. (b) Plot of [Mg] + [Fe] vs. [Nb] + [Ta]. Both data sets have a slope of approximately 1:2, providing evidence for a columbite-like component in solid-solution (see text for statistics and further discussion).

unaltered, despite being subjected to irradiation by alpha-recoil nuclei and alpha-particles emitted by the associated uranpyrochlore.

3.5. Radiation damage effects

Using Eqs. (1) and (2), the measured U concentrations of baddeleyite were used to calculate an alpha dose range of 0.0–0.09 $\times$ 10^{16} mg^{-1}, equivalent to 0.02–0.09 dpa based on the assumption that there are 1500 displacements per alpha-decay event. This assumption was investigated further using the software package TRIM [37]. Results of the calculations are displayed graphically in Fig. 4. The data suggest that the above assumption is only reasonable for an average value of E_d close to 20 eV. Higher average values of E_d significantly reduce the total number of displacements per alpha-decay event (Fig. 4). Unfortunately, there are no reliable measurements of the displacement energies of Zr and O in baddeleyite or any other zirconium oxide or silicate phase. A recent review article by Weber et al. [38] indicates that E_d ranges from 20 to 55 eV for metal cations and from 20 to 70 eV for oxygen in several simple oxide structures. The average displacement energies of these compounds range from 27 to 48; therefore, based on the TRIM simulations (see Fig. 4) the calculated dpa values reported above may be overestimated by about a factor of approximately 1.5–2.5.

TEM results demonstrate that the internal alpha-decay damage has had very little effect on the crystallinity and microstructure of the natural baddeleyite. A representative bright field image taken from the core of one of the baddeleyite crystals is shown in Fig. 5(a). This image and others like it show none of the microstructural features typical of the crystalline–amorphous transformation documented previously for a number of oxide and silicate phases [10,39,40]. Likewise, the zone axis electron diffraction patterns are sharp (Fig. 5(a), inset) and there is no evidence for the presence of a diffuse ring, even when the crystal is tilted away from the zone axis diffraction condition. The cumulative dose of the baddeleyite core region is near the beginning of the crystalline–amorphous transformation in other minerals (e.g., pyrochlore, zirconolite and zircon), suggesting that baddeleyite may be more resistant to alpha-decay

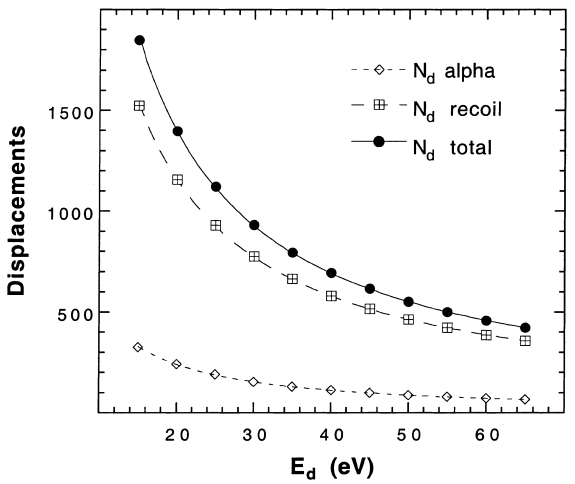

Fig. 4. Plot of the average number of displacements per ion in baddeleyite based on TRIM simulations. Total displacements and individual displacements for the 4.185 MeV alpha-particle and 72 keV ^{234}Th recoil atom from the decay of ^{238}U are plotted versus the average displacement energy, E_d. This figure illustrates the need for accurate measurements of E_d for actinide host phases in ceramic nuclear waste and fuel materials.

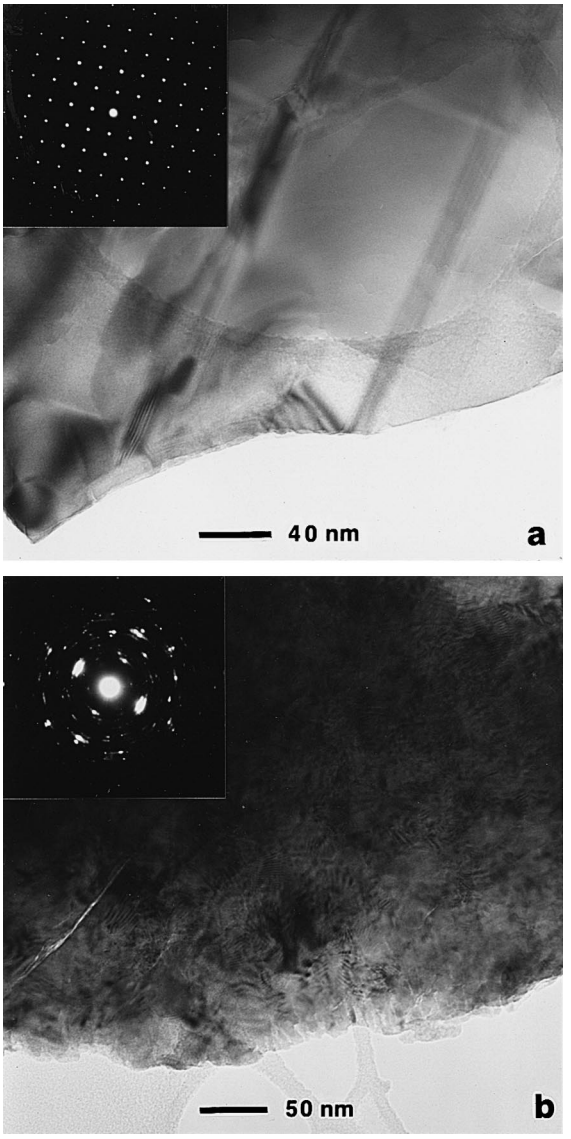

Fig. 5. Representative TEM images and selected area diffraction patterns from the core (a) and rim (b) of a baddeleyite crystal from Jacupiranga, Brazil. (a) Bright field image of the core shows evidence for twinning and limited subgrain development near the lower left edge of the crystal, but there is no convincing evidence for radiation damage (e.g., mottled diffraction contrast); electron diffraction pattern (inset) taken down [0 0 1] does not contain diffuse rings. (b) Bright field image of the rim shows evidence for extensive formation of a domain structure. Numerous fine modulations are also evident in parts of the image. Electron diffraction pattern (inset) consists of a spotty ring pattern, consistent with misalignment of up to 25° between domains in the plane of view.

damage, but it is difficult to make any further assessment of the data, especially since the dpa values may be an overestimate.

A secondary source of damage exists for the baddeleyite grains intergrown with uranpyrochlore. In this case, the baddeleyite will have received an additional alpha-decay dose from the adjacent uranpyrochlore crystals. The additional dose received by the baddeleyite decreases from 50% of the dose of the uranpyrochlore at the grain boundary down to zero just beyond the maximum depth of penetration for recoil atoms and alpha-particles. TRIM simulations indicate that the recoil atoms will penetrate to approximately 19 nm and that the alpha-particles will penetrate to just over 10 μm on average. The associated uranpyrochlore crystals generally contain 19–26 wt% UO_2 and 0.3–3.5 wt% ThO_2, from which an alpha dose range of $6–9 \times 10^{16}$ mg^{-1} is calculated. Therefore, the alpha-decay dose of the adjacent baddeleyite ranges from $3–4.5 \times 10^{16}$ mg^{-1} at the grain boundary down to the internally generated value of $0.02–0.09 \times 10^{16}$ mg^{-1} at the maximum depth of penetration calculated for the two projectiles.

Regions of baddeleyite close to the grain boundary were also investigated by TEM. Bright field images and diffraction patterns indicate that these areas have developed a modified microstructure characterized by heavily strained and rotated crystalline domains. The diffraction pattern shown in the inset of Fig. 5(b) provides a typical example and indicates that the maximum degree of rotation of the domains is about 25°. The bright field image (Fig. 5(b)) exhibits unusual mottled contrast features and fine scale modulation. Measurements using dark field images indicate that the domain size is on the order of 5–20 nm and that the fine scale modulation is approximately 1 nm. There is little evidence for the formation of amorphous domains in these areas of baddeleyite near the grain boundary, as shown by the lack of diffuse rings in the diffraction pattern. These observations are generally consistent with ion irradiation studies of cubic zirconia solid-solutions which develop defect clusters after 60 keV Xe irradiation or high density dislocation loops after 1.5 MeV Xe irradiation, but do not exhibit any sign of amorphization at doses up to 25 dpa [20]. However, the microstructure of the natural sample indicates that defect mobility may be significant over long periods of time, leading to the development of misaligned crystalline domains.

4. Discussion and conclusions

The results of this review and case study indicate that baddeleyite, like zirconolite [22,41], is a widespread but rare mineral in nature. The range of stability may be extensive in terms of temperature and pressure, but baddeleyite is largely restricted to silica poor bulk rock compositions. There is some evidence for the reaction of baddeleyite with silica bearing aqueous fluid to form zircon at moderate to low temperatures; however, the

degree of reaction appears to decrease with temperature [21], indicating that the durability is dominated by kinetic factors at very low temperatures. Isotopic studies also demonstrate that baddeleyite retains Th, U and Pb for geological time periods in excess of 2×10^9 yr. Results of the case study of baddeleyite from Jacupiranga, Brazil further emphasize the durability of the mineral in carbonatite systems. Under hydrothermal conditions, baddeleyite remained largely unaffected by an aqueous fluid phase that caused alteration in associated uranpyrochlore crystals.

Very few accurate analyses have been published for baddeleyite samples, primarily due to the rarity and fine grain size of the mineral in natural environments. The existing data indicate that Ti, Fe and Hf are the major impurities in the natural samples, with lesser amounts of Y, Nb and other elements. Total actinides are generally below 2000 ppm, but can result in cumulative alpha-decay doses of up to 1×10^{16} mg^{-1} for samples with ages of up to 2×10^9 yr. In the present work, both SEM-EDX and EPMA analyses show that a significant amount of Nb is incorporated in baddeleyite from the Jacupiranga carbonatite. Incorporation of Nb into the structure is charge balanced mainly by Mg and Fe and statistical data provide strong evidence for the presence of a columbite-like chemical component in baddeleyite. The ability to incorporate Nb^{5+} suggests that ZrO_2 in fuel and waste matrices may be able to incorporate Np^{5+}, depending upon oxygen fugacity and crystal chemical factors. The ionic radius of Np^{5+} in eight fold coordination is 0.085 nm, as estimated from Ref. [42]. Although somewhat larger than the ionic radius of Nb^{5+} (0.074 nm), the radius of Np^{5+} compares favorably to that of Zr^{4+} (0.084 nm) and may be able to occupy the Zr-site with appropriate charge compensation.

The limited evidence from the literature suggests that baddeleyite may be more resistant to the effects of alpha-decay damage from ^{232}Th and ^{238}U atoms incorporated in dilute solid solution. This evidence is consistent with previous ion irradiation studies [32] and is also supported to a certain extent by the case study presented above. However, the TEM results described in the case study document the potential modification of the microstructure of baddeleyite under intense alpha-particle irradiation by an adjacent actinide-rich phase. In this example, the bombardment by alpha-particles apparently caused the development of a domain structure and fine scale modulations, but otherwise did not significantly degrade the crystallinity of the material (see Refs. [19,20]). Perhaps more importantly, this study demonstrates that baddeleyite is highly robust in the presence of aqueous fluids, even after alpha-particle irradiation up to a maximum alpha dose of about 4.5×10^{16} mg^{-1}. In general, the results of this study indicate that monoclinic ZrO_2 with low levels of impurities will be a chemically durable and radiation resistant component of nuclear waste forms (e.g., tailored ceramics).

5. Recommendations for future work

During the course of this investigation, a number of areas have been identified where further work would be beneficial. These areas include: (1) an examination of the chemical composition and stoichiometry of baddeleyite in different geological environments, (2) careful studies of the paragenesis and geochemical alteration effects in natural samples as a function of temperature, pressure and fluid composition, (3) experimental studies of the durability of baddeleyite and stabilized ZrO_2 solid solutions under different conditions and as a function of radiation damage and (4) detailed investigations of the effects of radiation damage and dose rate on the crystallinity and microstructure of baddeleyite-stabilized ZrO_2 solid solutions using natural samples, actinide doping experiments and ion irradiation simulations.

Acknowledgements

I am sincerely indebted to the staff of the Materials Characterisation Section at ANSTO and the Department of Geological Sciences at the Universtity of New Mexico for their contributions to natural analogue studies carried out over the past 15 yr. In particular, I would like to thank George Conrad, Mark Blackford and Sammy Leung for their assistance with the electron microscopy and microanalysis aspects of this work. I would also like to thank Ken Kietzke, Darren Attard and Ted Roach for preparation of polished sections.

References

[1] A.B. Harker, in: W. Lutze, R.C. Ewing (Eds.), Radioactive Waste Forms for the Future, North-Holland, Amsterdam, 1988, p. 335.
[2] P.J. Hayward, in: W. Lutze, R.C. Ewing (Eds.), Radioactive Waste Forms for the Future, North-Holland, Amsterdam, 1988, p. 427.
[3] R.C. Ewing, in: W. Lutze, R.C. Ewing (Eds.), Radioactive Waste Forms for the Future, North-Holland, Amsterdam, 1988, p. 589.
[4] R.L. Garwin, in: W.M. Murphy, D.A. Knecht (Eds.). Scientific Basis for Nuclear Waste Management XIX, Mater. Res. Symp. Proc. 412 (1996) 3.
[5] T. Muromura, Y. Hinatsu, J. Nucl. Mater. 151 (1987) 55.
[6] E.R. Vance, Mater. Res. Soc. Bull. 19 (1994) 28.
[7] E.R. Vance, B.D. Begg, R.A. Day, C.J. Ball, in: T. Murakami, R.C. Ewing (Eds.), Scientific Basis for Nuclear Waste Management XVIII, Mater. Res. Symp. Proc. 353 (1995) 767.

[8] E.R. Vance, A. Jostsons, R.A. Day, C.J. Ball, B.D. Begg, P.J. Angel, in: W.M. Murphy, D.A. Knecht (Eds.), Scientific Basis for Nuclear Waste Management XIX, Mater. Res. Symp. Proc. 412 (1996) 41.
[9] C. Degueldre, U. Kasemeyer, F. Botta, G. Ledergerber, in: W.M. Murphy, D.A. Knecht (Eds.), Scientific Basis for Nuclear Waste Management XIX, Mater. Res. Symp. Proc. 412 (1996) 15.
[10] G.R. Lumpkin, K.P. Hart, P.J. McGlinn, T.E. Payne, R. Gieré, C.T. Williams, Radiochim. Acta 66&67 (1994) 469.
[11] G.R. Lumpkin, R.C. Ewing, Am. Mineral 81 (1996) 1237.
[12] R. Gieré, C.T. Williams, G.R. Lumpkin, in: I.G. McKinley, C. McCombie (Eds.), Scientific Basis for Nuclear Waste Management XXI, Mater. Res. Symp. Proc. 506 (1998) 1031.
[13] E.C. Subbarao, in: A.H. Heuer, L.W. Hobbs (Eds.), Science and Technology of Zirconia, Adv. Ceram. 3 (1981) 1.
[14] V.S. Stubican, J.R. Hellmann, in: A.H. Heuer, L.W. Hobbs (Eds.), Science and Technology of Zirconia, Adv. Ceram. 3 (1981) 25.
[15] S. Suzuki, M. Tanaka, M. Ishigame, J. Phys. C 20 (1987) 2963.
[16] T.R. Welberry, R.L. Withers, J.G. Thompson, B.D. Butler, J. Solid State Chem. 100 (1992) 71.
[17] R. Miida, M. Tanaka, H. Arashi, M. Ishigame, J. Appl. Crystallogr. 27 (1994) 67.
[18] F.W. Clinard Jr., D.L. Rohr, W. Ranken, J. Am. Ceram. Soc. 60 (1977) 287.
[19] E.R. Vance, J.N. Boland, Radiat. Eff. 37 (1978) 237.
[20] C. Degueldre, P. Heimgartner, G. Ledergerber, N. Sasajima, K. Hojou, T. Muromura, L. Wang, W. Gong, R. Ewing, in: T. Diaz de la Rubia, G.S. Was, I.M. Robertson, L.W. Hobbs, (Eds.), Microstructure Evolution During Irradiation, Mater. Res. Symp. Proc. 439 (1997) 625.
[21] L.M. Heaman, A.N. LeCheminant, Chem. Geol. 110 (1993) 95.
[22] C.M. Allen, D.J. Ellis, Stability of Zirconolite and its Occurrence in the Crustal Environment. A report for ANSTO, May 1996, Department of Geology, The Australian National University, Canberra, ACT, p. 26.
[23] S.E. Haggerty, in: D.H. Lindsley (Ed.), Oxide Minerals: Petrologic and Magnetic Significance, Rev. Mineral. 25 (1991) 355.
[24] Yu.L. Kapustin, Mineralogy of Carbonatites, Amerind, New Delhi, 1980, p. 259.
[25] G.N. Eby, A.N. Mariano, J. South Am. Earth Sci. 6 (1992) 207.
[26] C.M. Allen, D.J. Ellis, A Theoretical Analysis of the Stability and Phase Relations Involving Zirconolte in the $CaO–ZrO_2–TiO_2–SiO_2–CO_2$ System Under Crustal and Upper Mantle Conditions. A report for ANSTO, July 1996, Department of Geology, The Australian National University, Canberra, ACT, p. 28.
[27] H.G.F. Winkler, Petrogenesis of Metamorphic Rocks, 5th ed., Springer, New York, 1979, p. 348.
[28] S.C. Eriksson, Isotope Geosci. 2 (1984) 291.
[29] L.M. Heaman, J.P. Grotzinger, Geology 20 (1992) 637.
[30] J.G. Patterson, L.M. Heaman, Geology 19 (1991) 1137.
[31] A. Davidson, O. van Breemen, Contrib. Mineral. Petrol 100 (1988) 291.
[32] H.M. Naguib, R. Kelly, Radiat. Eff. 25 (1975) 1.
[33] Y.M. Huang, C.J. Hawkesworth, P. van Calsteren, F. McDermott, Chem. Geol. 119 (1995) 79.
[34] G.R. Lumpkin, R.C. Ewing, Am. Mineral. 77 (1992) 179.
[35] G.R. Lumpkin, K.L. Smith, M.G. Blackford, R. Gieré, C.T. Williams, Micron 25 (1994) 581.
[36] G.R. Lumpkin, R.C. Ewing, Am. Mineral. 80 (1995) 732.
[37] J.F. Ziegler, J.P. Biersack, U. Littmark, The Stopping and Range of Ions in Solids, Pergamon, New York, 1985.
[38] W.J. Weber, R.C. Ewing, C.R.A. Catlow, T. Diaz de la Rubia, L.W. Hobbs, C. Kinoshita, Hj. Matzke, A.T. Motta, M. Nastasi, E.K.H. Salje, E.R. Vance, S.J. Zinkle, J. Mater. Res. (1998) 1434.
[39] G.R. Lumpkin, R.C. Ewing, Phys. Chem. Miner. 16 (1988) 2.
[40] T. Murakami, B.C. Chakoumakos, R.C. Ewing, G.R. Lumpkin, W.J. Weber, Am. Mineral. 76 (1991) 1510.
[41] R. Gieré, C.T. Williams, G.R. Lumpkin, Schweiz. Mineral. Petrogr. Mitt. 78 (1998) 433.
[42] R.D. Shannon, Acta Crystallogr. A 32 (1976) 751.